CHAPTER 6

RESULTS

6.1 Controller Implementation and Organization of Results

The three controller schemes, designed in chapter 5, were discretized first before they were implemented on the nonlinear simulator.

The discretization for the diagonal controller was done, by using the velocity form to compute the controller outputs. A model reduction was performed on the continuous state space matrices of the H_∞ controllers for the second linear model. Its number of states was reduced from 9 to 7.

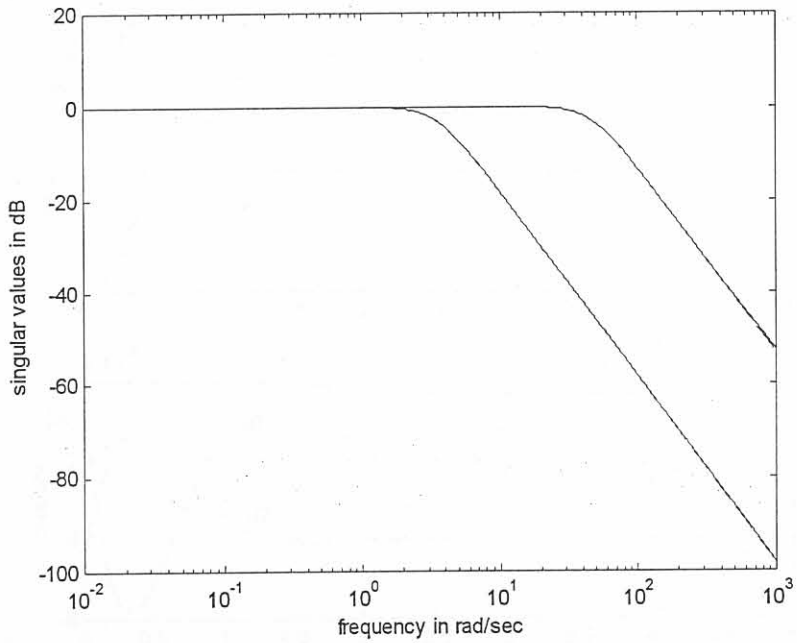

Figure 6.1: Closed-loop singular values of the H_∞ controller for the second linear model (dashed) and of the model reduced H_∞ controller for the second linear model (solid).

Fig. 6.1 compares the closed-loop singular value of the reduced to the unreduced controller. From this figure it can be seen that the singular values of the closed loops with the reduced and original controllers differ only at higher frequencies.

The time domain simulations for a set point $r = [3e-4 \quad 0 \quad 0]$ in figures 6.2 through 6.5 show a more severe interaction between the control actions and system outputs in the case of the model reduced controller. However figures 6.2 through 6.7 show that the model reduced controller and the unreduced controller are capable of performing equally well. In figures 6.2 through 6.5 only two outputs and control actions are shown on each graph although three set points were given for each. This was done because only two different scales were available for the ordinate of each graph. However all outputs and control actions for the H_∞ controller for the second linear model and the model reduced controller for the second linear model are covered. In Figures 6.6 and 6.7 all three outputs and controller actions are plotted but those with zero set points cannot be distinguished from each other because they lie on the same lines.

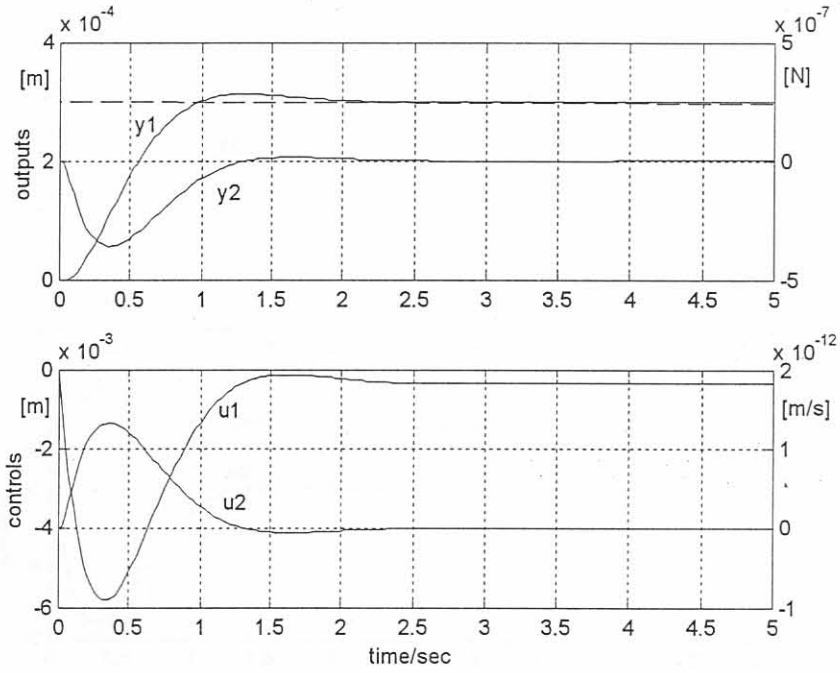

Figure 6.2: Closed-loop simulation results of the H_∞ controller and the second linear model for the set point r = [3e-4 0 0] – (SI units apply).

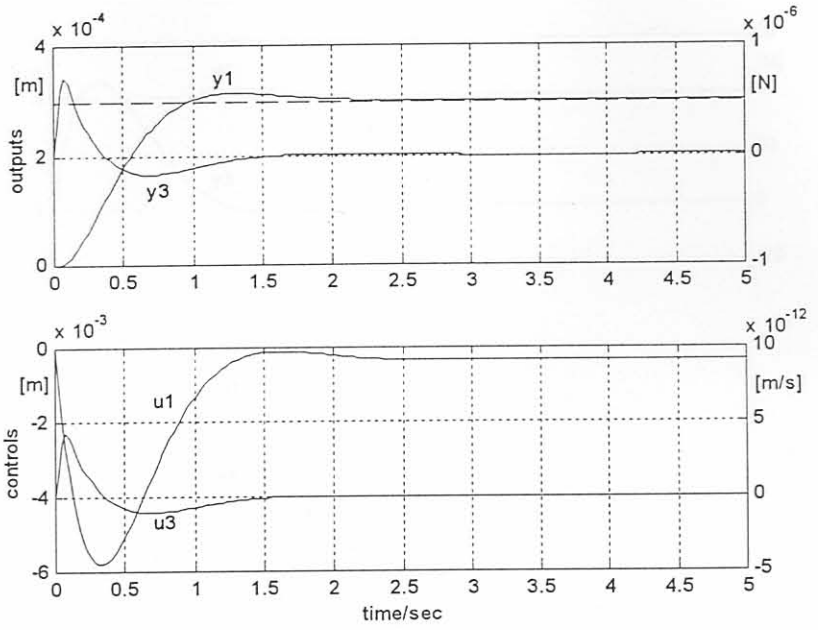

Figure 6.3: Closed-loop simulation results of the H_∞ controller and the second linear model for the set point r = [3e-4 0 0] – (SI units apply).

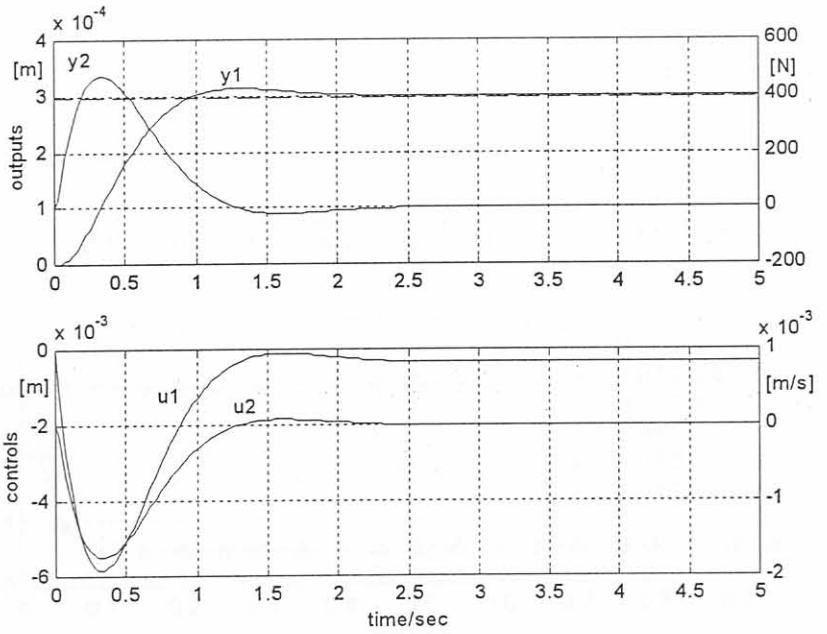

Figure 6.4: Closed-loop simulation results of model-reduced H_∞ controller and the second linear model for the set point r = [3e-4 0 0] – (SI units apply).

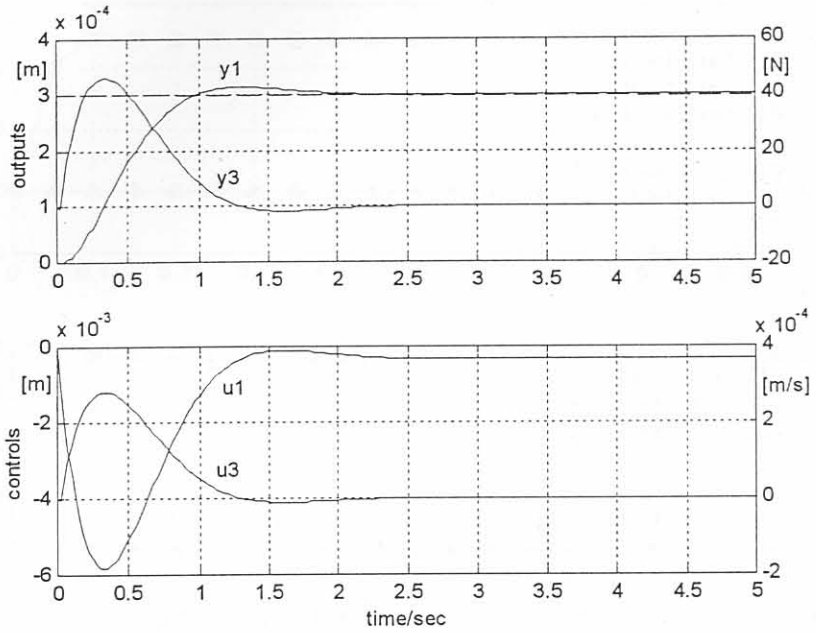

Figure 6.5: Closed-loop simulation results of the model-reduced H_∞ controller and the second linear model for the set point r = [3e-4 0 0] – (SI units apply).

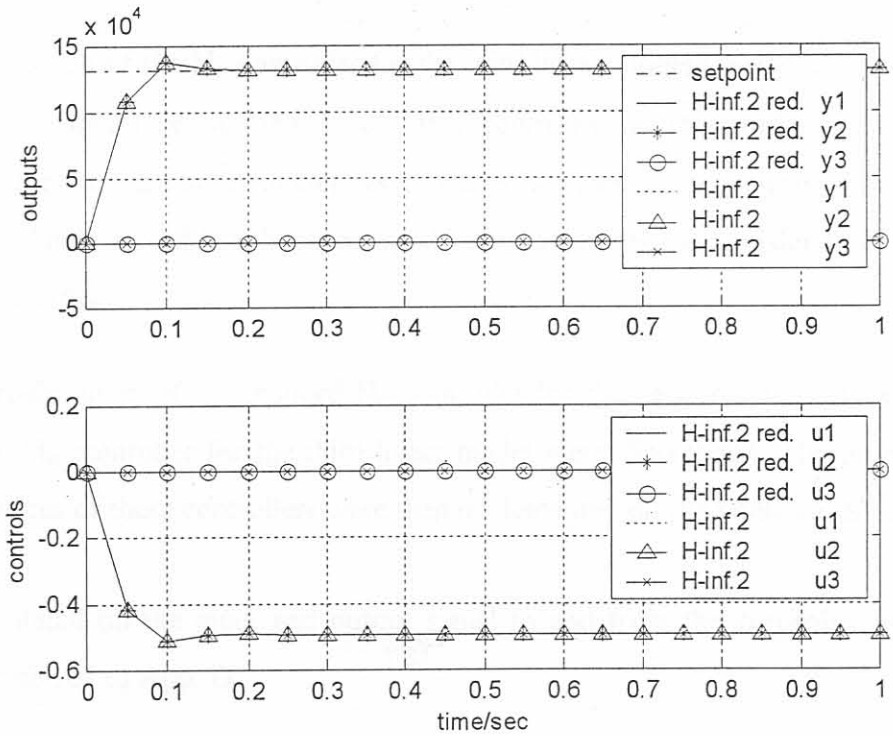

Figure 6.6: Closed-loop simulation results of an H_∞ controller with the second linear model and model-reduced H_∞ controller with the second linear model for the set point r = [0 1.32e5 0] – (SI units apply).

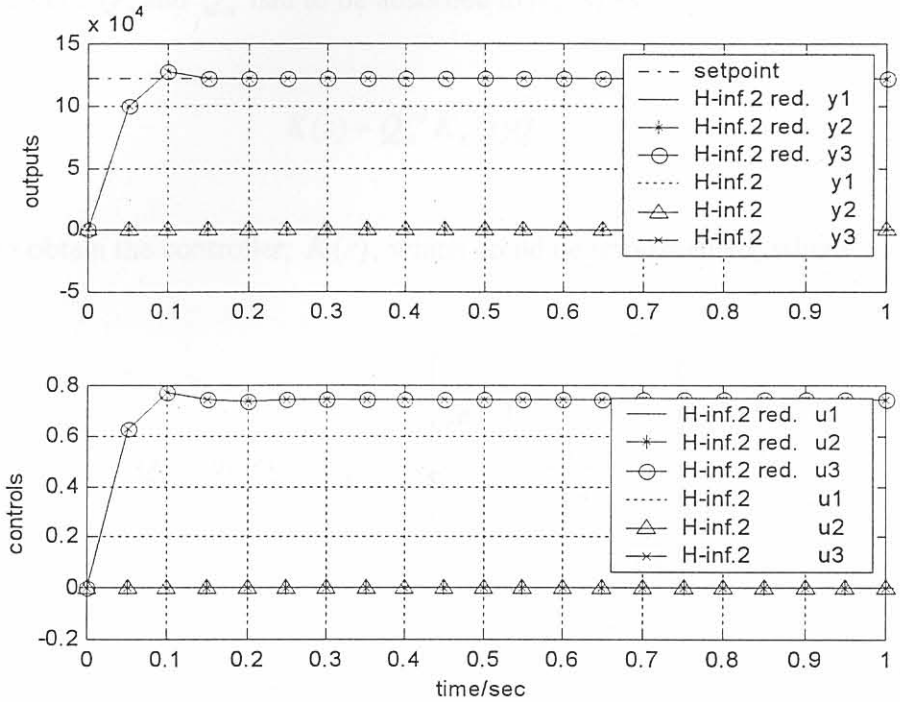

Figure 6.7: Closed-loop simulation results of an H_∞ controller with the second linear model and the model-reduced H_∞ controller with the second linear model for the set point r = [0 0 1.22e5] – (SI units apply).

Model reduction of the H_∞ controller for the third linear model yielded an unstable closed-loop. It was therefore decided to use this controller in its unreduced form. The H_∞ controller for the third linear model has 19 states, which is more than the H_∞ controller for the second linear model has, because the third linear model has transfer function elements with higher orders.

Minimal realizations of the reduced H_∞ controller for the second linear model and of the unreduced H_∞ controller for the third linear model were discretized. The discretized state space matrices of these controllers were then implemented on the nonlinear simulator.

For more detail on the input and output signal to and from the controller and plant the reader is referred to App. D.

Because the H_∞ controllers, $K_s(s)$, were designed for a scaled plant,

$$G_s(s) = Q_y G(s) Q_u^{-1}, \tag{6.1}$$

scaling matrices Q_y and Q_u had to be absorbed in $K_s(s)$ as

$$K(s) = Q_u^{-1} K_s(s) Q_y \quad , \tag{6.2}$$

in order to obtain the controller, $K(s)$, which could be implemented, where

$$Q_u = diag[1/u_{j\max}] = \begin{bmatrix} \frac{1}{1e-3} & 0 & 0 \\ 0 & \frac{1}{0.4} & 0 \\ 0 & 0 & \frac{1}{0.4} \end{bmatrix} \tag{6.3}$$

and

$$Q_y = diag[1/y_{j\max}] = \begin{bmatrix} \frac{1}{3e-4} & 0 & 0 \\ 0 & \frac{1}{2e6} & 0 \\ 0 & 0 & \frac{1}{0.5e6} \end{bmatrix}. \tag{6.4}$$

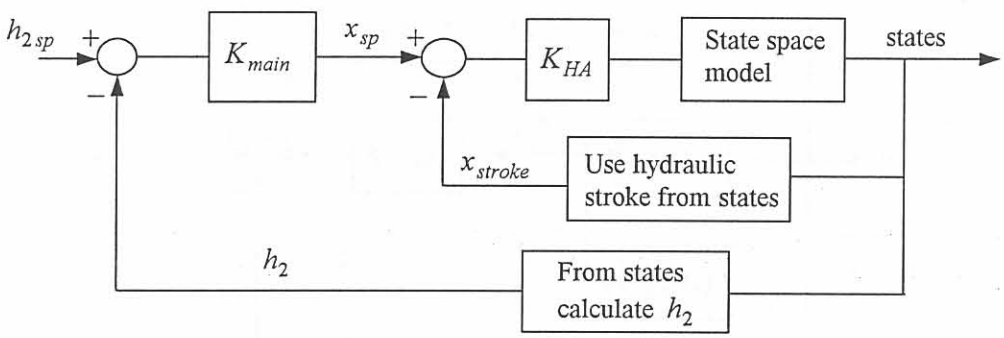

Figure 6.8: Control action of designed controller schemes applied to hydraulic actuator control loop.

Fig. 6.8 shows how the controller action, $u_1 = x_{sp}$ (hydraulic stroke set point) of the diagonal or H_∞ controllers, indicated by K_{main}, are applied to the simulator. Seen in isolation from the exit gauge /tension interactions the block diagram in this figure shows

that the feedback loop of the output, y_1, which is exit gauge, h_2, yields a cascade structure, when controlled by the diagonal or H_∞ control action, u_1. In this figure K_{HA} represents the hydraulic actuator PI controller.

For the controller implementation on a plant with inner loop tension control, such as for the second and third linear model, the scheduling of the inner loop tension control and H_∞ controller action is illustrated in Fig. 6.9 for back tension control. This scheduling is implemented such that the tensions are controlled by PI controllers of the inner loop tension control after every time step of length Δt_{main} where $\Delta t_{tension} < \Delta t_{main}$. This means that inner loop tension control actions are applied at a higher frequency than the H_∞ control actions. The summation of the H_∞ control action and the previous PI control action of the inner loop tension control is done in order to bring the control action of the H_∞ controller close to the control action of the PI controllers, which do most of the manipulating work on the plant tension outputs.

The same configuration, as in Fig. 6.9, applies to front tension control.

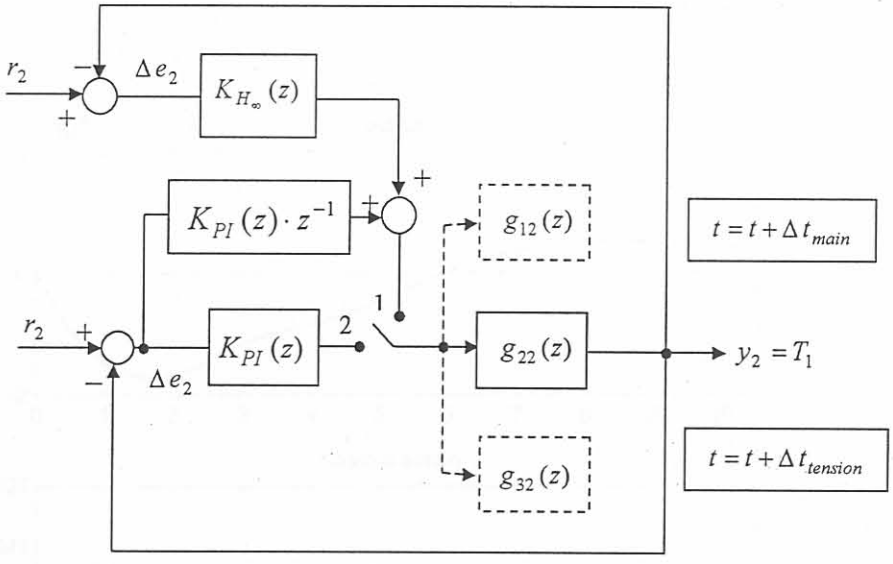

If Δt_{main} multiple of t : switch position 1
else : switch position 2

with $\Delta t_{tension} < \Delta t_{main}$

Figure 6.9: Control action scheduling of H_∞ and inner loop tension controller.

The results that are presented in this chapter's sections to follow were all simulated with a step set point change of the front tension from 10 N to its set up value. This kind of set point change occurs at the beginning of a pass when the tensions are established [41]. In particular section 6.2 contains the results when a diagonal controller scheme was applied to the nonlinear plant without inner loop tension control and gauge meter compensation. Sections 6.3 and 6.4 show results from simulations with H_∞ controllers implemented on a plant which did incorporate inner loop tension control and gauge meter compensation, where the difference between the latter two H_∞ controllers lies in the linear models on which their designs were based, i.e. the second and third linear model. In a discussion of the results in section 6.5 the three controllers are compared. The chapter is concluded with some words about the context of the controller design.

6.2 Results of Diagonal Controller Implementation on Nonlinear Simulator

The results presented in this section are from a simulation of the nonlinear plant in closed loop with the diagonal PID controller of which the design was discussed in section 5.3.

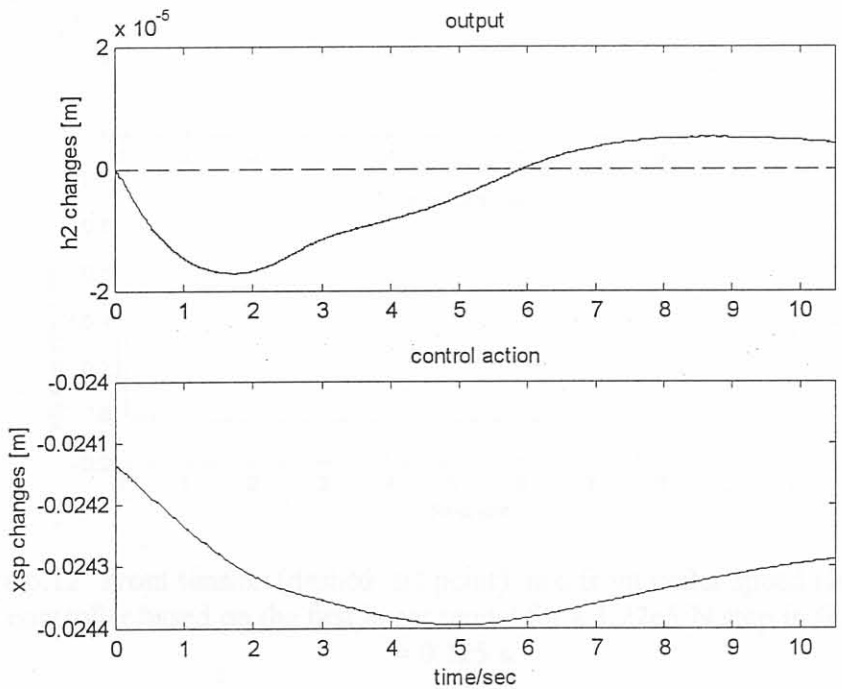

Figure 6.10: Exit gauge changes (dashed: set point) and hydraulic actuator stroke set point changes for a diagonal controller based on first linear model for a 1.22e5 N step in front tension at t = 0.125 s.

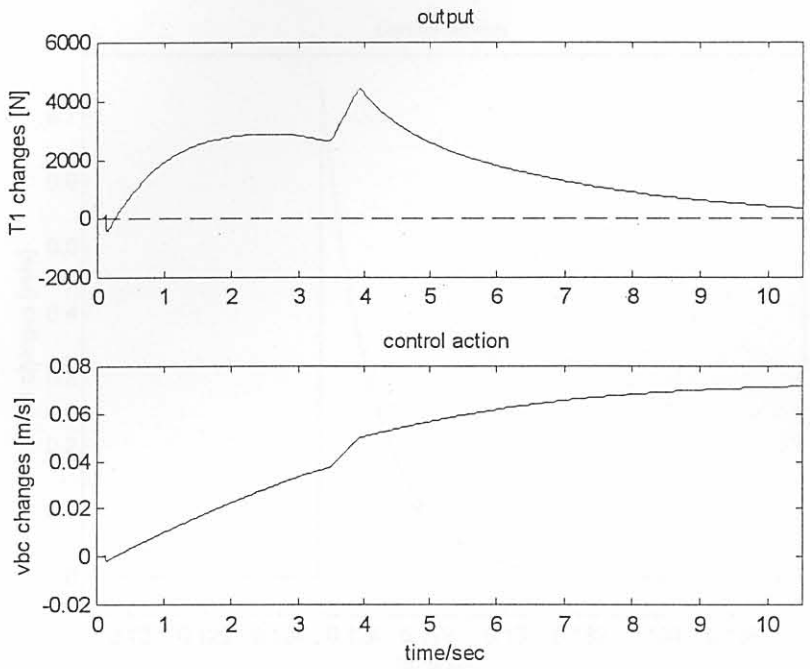

Figure 6.11: Back tension changes (dashed: set point) and back coiler speed changes for a diagonal controller based on the first linear model for a 1.22e5 N step in front tension at t = 0.125 s.

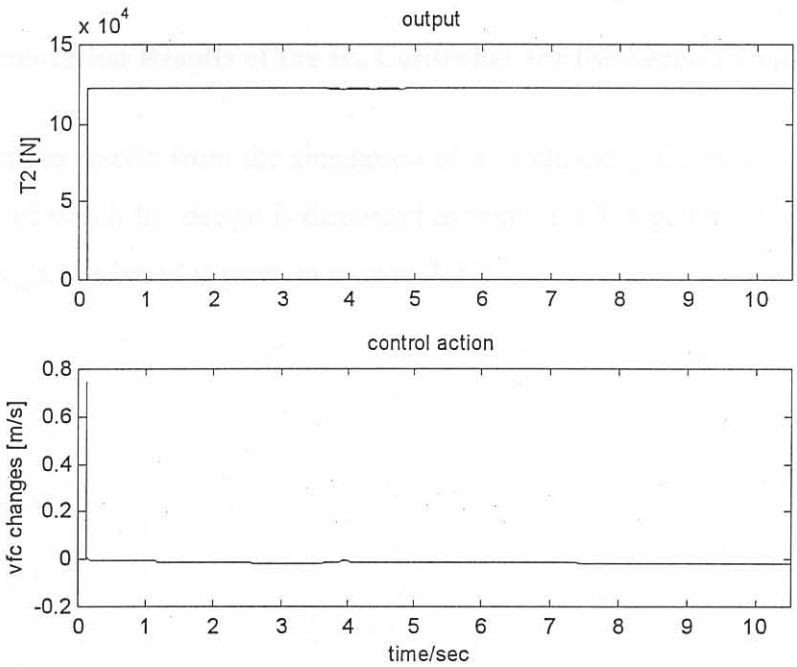

Figure 6.12: Front tension (dashed: set point) and front coiler speed changes for a diagonal controller based on the first linear model for a 1.22e5 N step in front tension at t = 0.125 s.

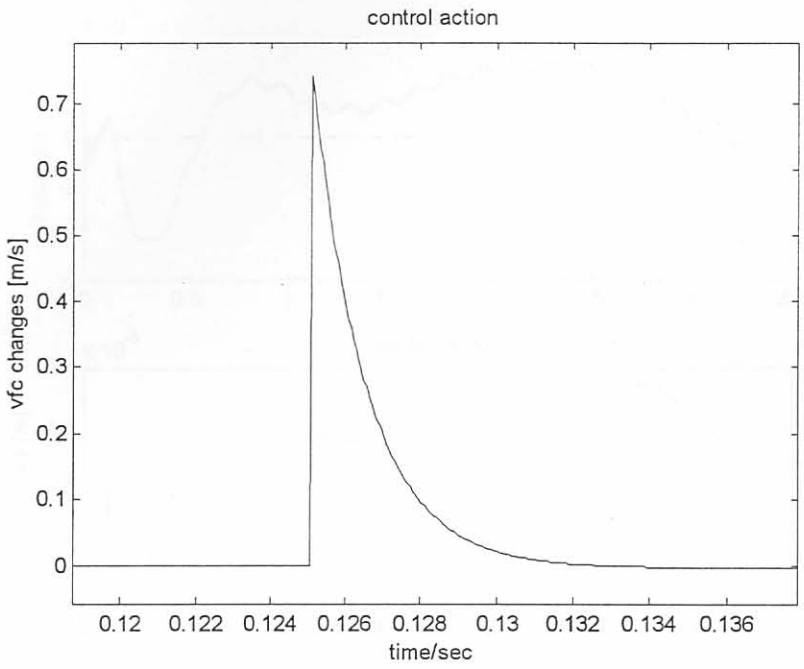

Figure 6.13: Control action (front coiler speed changes) of diagonal controller based on first linear model for a 1.22e5 N step in front tension at t = 0.125 s.

6.3 Implementation Results of the H_∞ Controller for the Second Linear Model

In this section the results from the simulation of a nonlinear plant in closed loop with an H_∞ controller of which the design is discussed in section 5.5 is given. The linear model on which this design was based is given in section 3.4.2.

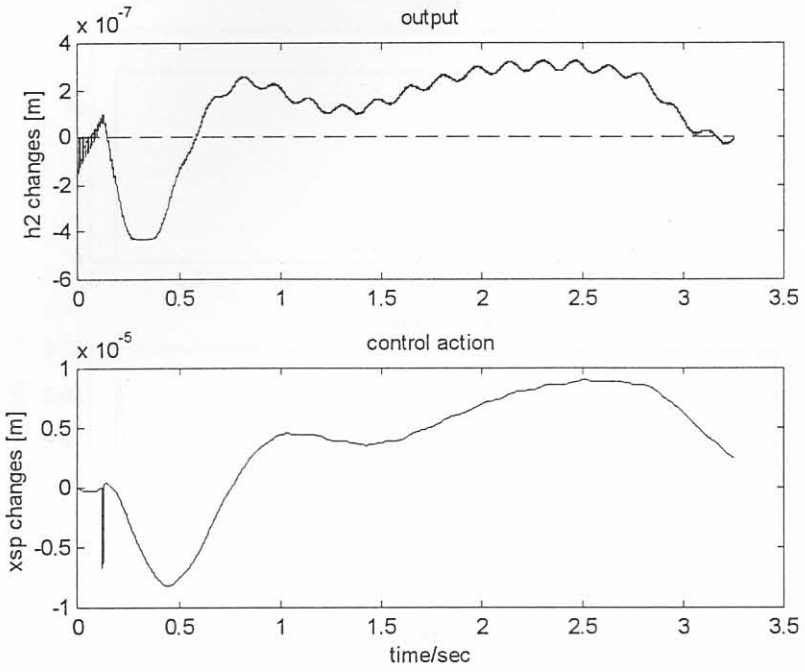

Figure 6.14: Exit gauge changes (dashed: set point) and hydraulic actuator stroke set point changes for the H_∞ controller based on the second linear model for a 1.22e5 N step in front tension at t = 0.125 s.

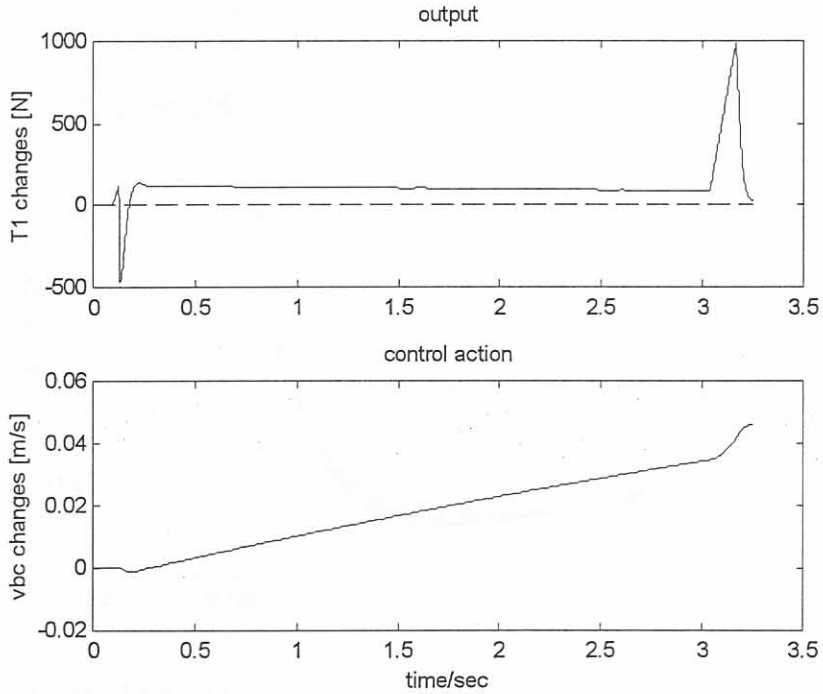

Figure 6.15: Back tension changes (dashed: set point) and back coiler speed changes for the H_∞ controller based on the second linear model for a 1.22e5 N step in front tension at t = 0.125 s.

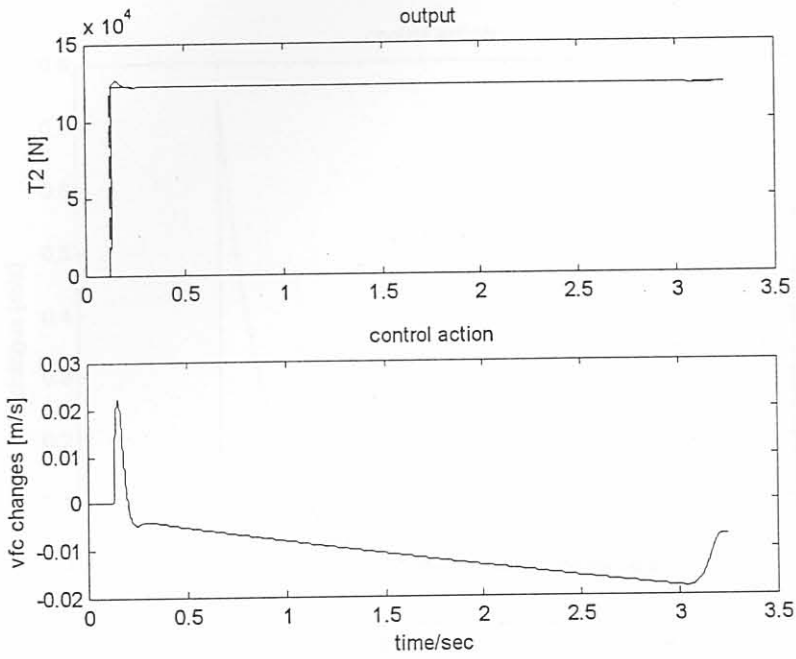

Figure 6.16: Front tension (dashed: set point) and front coiler speed changes for the H_∞ controller based on the second linear model for a 1.22e5 N step in front tension at t = 0.125 s.

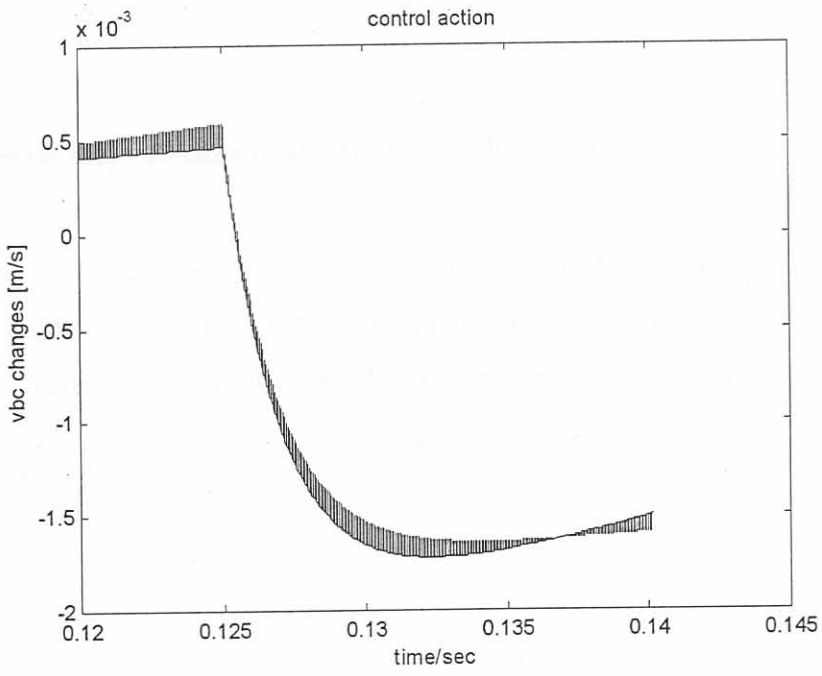

Figure 6.17: Control action (back coiler speed changes) of inner loop tension control for the H_∞ controller based on the second linear model for a 1.22e5 N step in front tension at t = 0.125 s.

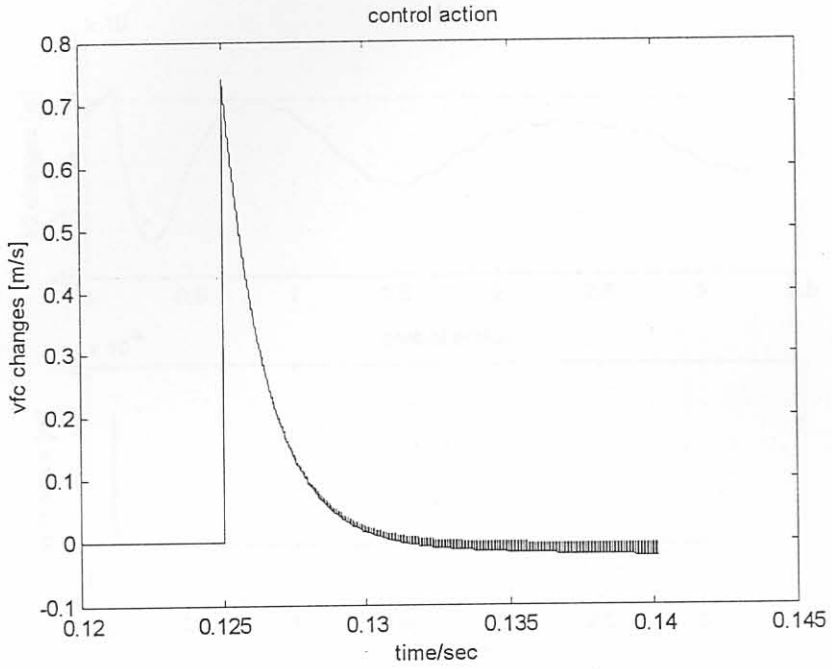

Figure 6.18: Control action (front coiler speed changes) of inner loop tension control for the H_∞ controller based on the second linear model for a 1.22e5 N step in front tension at t = 0.125 s.

6.4 Implementation Results of the H_∞ Controller for the Third Linear Model

The nonlinear plant used for the simulations of which the results are presented in this section, had inner loop tension control and gauge meter compensation incorporated in it. The design of the H_∞ controller in closed loop with this plant was given in section 5.6.

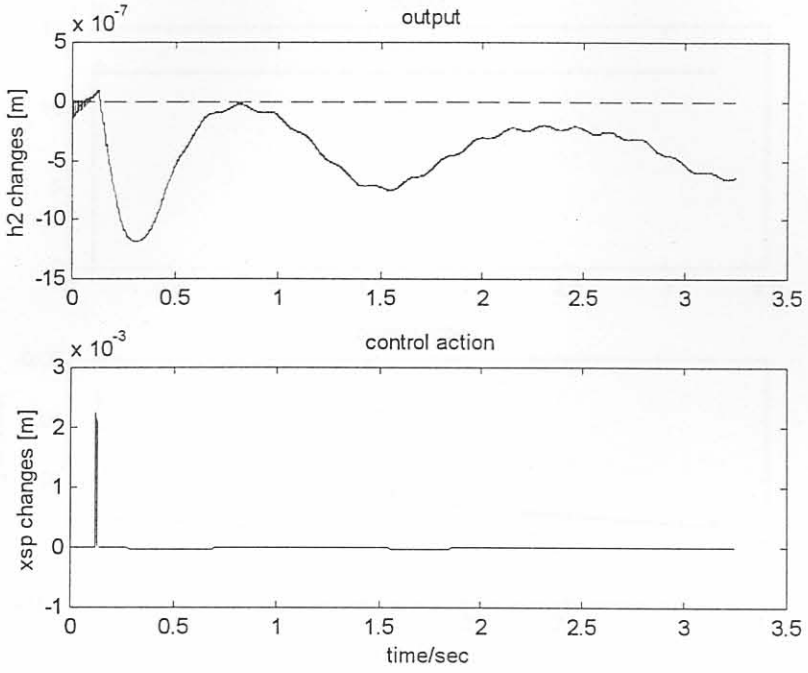

Figure 6.19: Exit gauge changes (dashed: set point) and hydraulic actuator stroke set point changes for the H_∞ controller based on the third linear model for a 1.22e5 N step in front tension at t = 0.125 s.

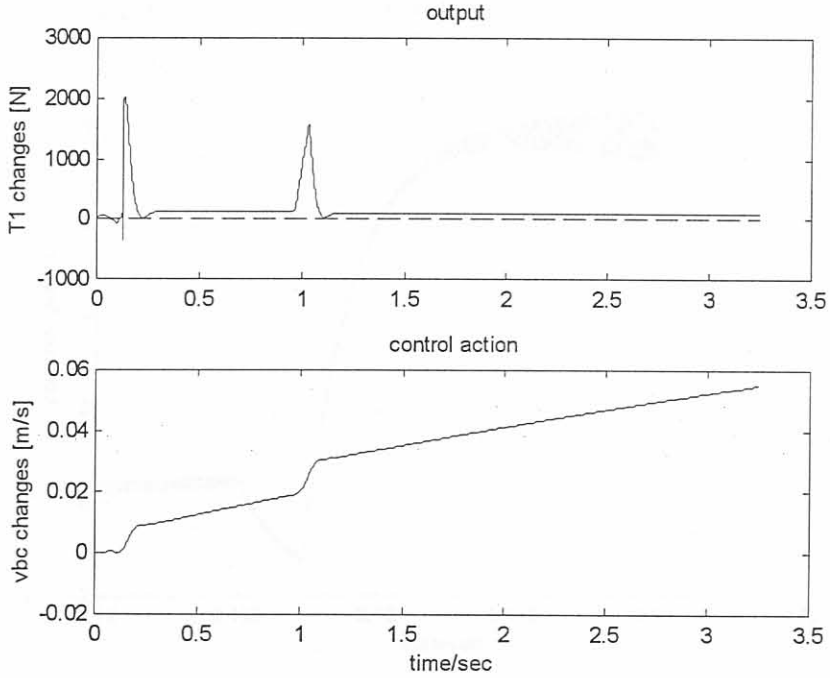

Figure 6.20: Back tension changes (dashed: set point) and back coiler speed changes for the H_∞ controller based on the third linear model for a 1.22e5 N step in front tension at t = 0.125 s.

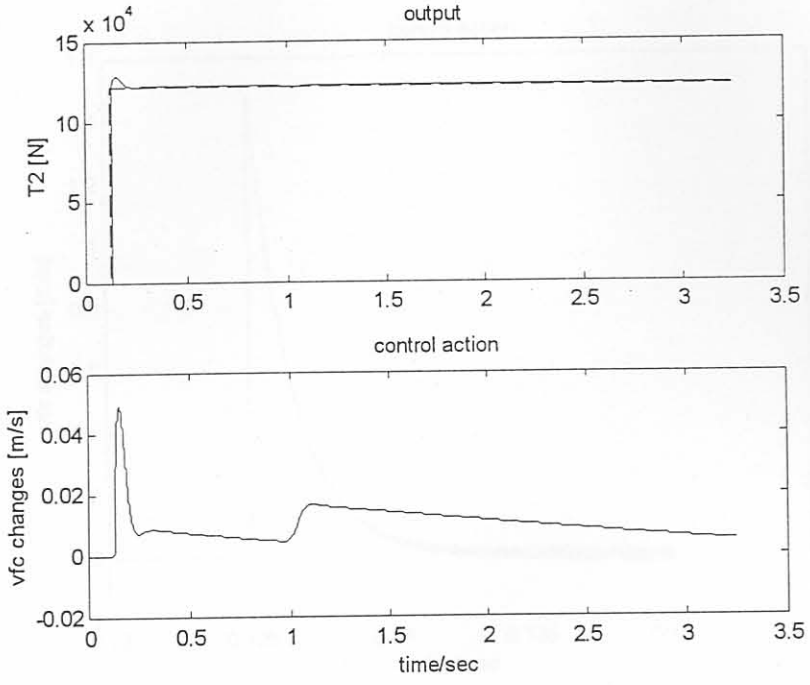

Figure 6.21: Front tension (dashed: set point) and front coiler speed changes for the H_∞ controller based on the third linear model for a 1.22e5 N step in front tension at t = 0.125 s.

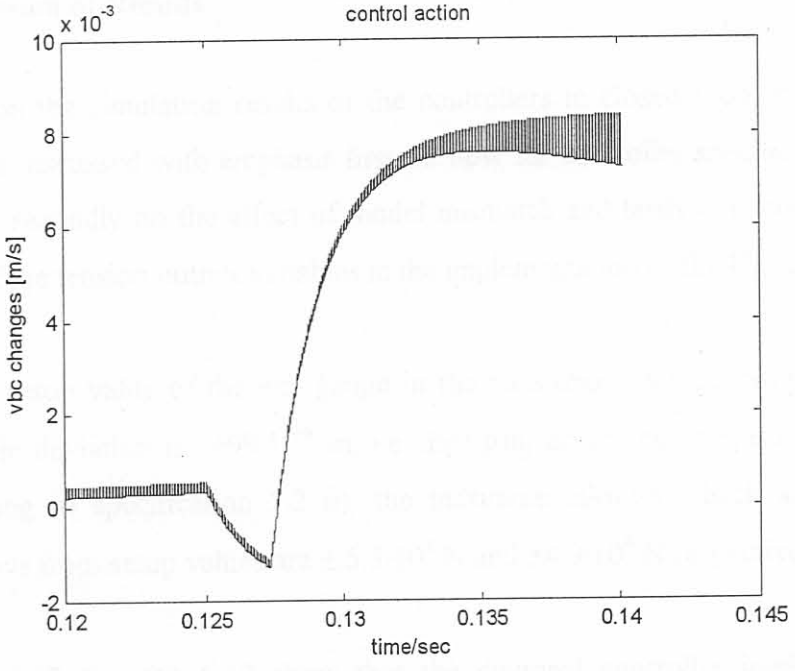

Figure 6.22: Control action (back coiler speed changes) of inner loop tension control for the H_∞ controller based on the third linear model for a 1.22e5 N step in front tension at t = 0.125 s.

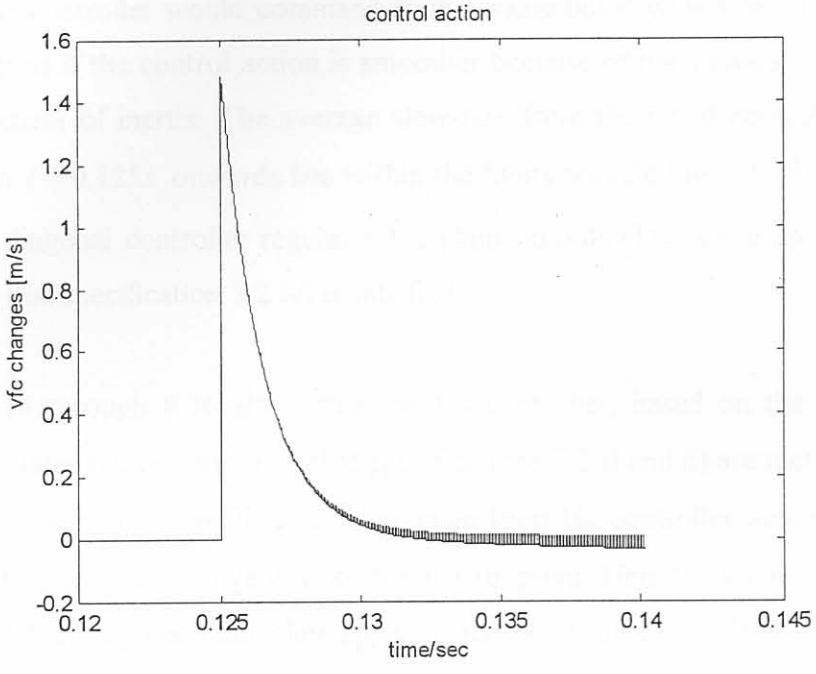

Figure 6.23: Control action (front coiler speed changes) of inner loop tension control for the H_∞ controller based on the third linear model for a 1.22e5 N step in front tension at t = 0.125 s.

6.5 Discussion of Results

In this section the simulation results of the controllers in closed loop with the nonlinear simulator are discussed with emphasis first on how far controller specifications in section 5.2 are met, secondly on the effect of model mismatch and lastly it is commented on the behaviour of the tension output variables in the implementation of the H_∞ controllers.

i) For the setup value of the exit gauge in the pass under consideration, the maximum allowable deviation is $\pm 99 \cdot 10^{-6}$ m, i.e. ±99 μm, according to specification i) in 5.2. According to specification 5.2 ii), the maximum allowable back and front tension deviations from setup values are $\pm 5.3 \cdot 10^4$ N and $\pm 4.9 \cdot 10^4$ N respectively.

Figures 6.10 through 6.12 show that the diagonal controller implemented on the nonlinear simulator meets specifications 5.2 i) and ii). The controller actions are shown on the same figures and also on Fig. 6.13. The curves representing the controller action, u_3, i.e. front coiler speed, in figures 6.12 and 6.13 have points in which derivatives are non-existent. These points can be attributed to the fact that the PI

controllers always have an initial value when implemented in the velocity form. In practice the controller would command such a value but it would result in a response of the plant as if the control action is smoother because of the slew-rate limited by the coilers moment of inertia. The average slew-rate from the initial control action value of u_3 from $t = 0.125s$ onwards lies within the limits specified in 5.2. iii). The way by which the diagonal controller regulates the plant outputs close to setup values, points to the fact that specification 5.2 iv) is satisfied.

Figures 6.14 through 6.16 show that the H_∞ controller, based on the second linear model, regulates the outputs such that specifications 5.2 i) and ii) are met. Figures 6.17 and 6.18 show inner loop PI as well as main loop H_∞ controller actions for tension control during the step change in front tension set point. Here the same arguments as in the case of the diagonal controller apply to the points in controller actions in which derivatives are non-existent. The average slew-rate for the control actions, $u_2 = v_{bc}$ and $u_3 = v_{fc}$ however lie within the limits specified. Again for this H_∞ controller scheme figures 6.14 through 6.16 show that 5.2 iv) is satisfied.

In figures 6.19 through 6.21 it can be seen that the H_∞ controller, which is based on the third linear model, regulates the plant outputs within the specified limits in 5.2 i) and ii). The slew-rate as shown in Fig. 6.22 can be obtained in practice however not the one shown in Fig.6.23. Here again points in control actions, u_2 and u_3, in which derivatives do not exist, are present. The same arguments, as mentioned in the case of the diagonal controller, apply to these points. The trends of the outputs in figures 6.19 through 6.21 show that specification 5.2 iv) is met for the duration of the simulation.

ii) The closed-loop simulation results with the nonlinear simulator show that model mismatch affects both, the diagonal controller and the H_∞ controller designed for the third linear model.

In the case of the diagonal controller, the PID controller, $k_{11}(s)$, was designed for a transfer function, $g_{11}(s)$, for which the tension model was excluded during SID, i.e. SID was performed on an incomplete model.

In the case of the H_∞ controller for the third linear model, the slew-rate of the controller action, u_3, is too high. This can be attributed to model mismatch. Model mismatch is weighing more for the controller based on the third linear model than for the controller based on the second linear model. This is so because from the transfer function $g_{31}(s)$ the controller for the third model is designed from the information that for a decrease in exit gauge, i.e. the input to $g_{31}(s)$, the front tension is lower than the average measured front tension (see Fig. 3.40). Therefore the tendency of this controller is to command a control action, u_3, which exceeds the limits specified in 5.2. iii), for a decrease in exit gauge.

iii) In the output data of transfer functions $g_{21}(s)$ and $g_{31}(s)$ nonlinear behaviour for hydraulic stroke step input in the case of the plant with inner loop tension control and gauge meter compensation (see figures 3.39 and 3.40) can be seen. It is the authors opinion that this nonlinear behaviour is reflected as spikes on the tension outputs when the plant is in closed loop with the H_∞ controllers designed for the second and third linear models. It could be that these spikes appear because this nonlinear behaviour has not been taken into account in the identification of the transfer functions, $g_{21}(s)$ and $g_{31}(s)$. This behaviour of $g_{21}(s)$ and $g_{31}(s)$ can be attributed to a disturbance due to exit gauge/tension interaction since the tensions are the controlled variables and the coiler speeds the manipulated variables when a plant with inner loop tension control is considered. A plant with inner loop tension control means that the integrator transfer functions, $g_{22}(s)$ and $g_{33}(s)$, from the first linear model are in closed loop with PI-controllers. Changes in exit gauge, such as during its steady state development, can therefore be seen as disturbances to the inner tension control loops.

6.6 Context and Evaluation of Controller Design

As point of linearization for the identification of a linear model an operating point was chosen on the speed up ramp of the rolling process. This model and consequently the controller design based on it are valid for only a small part for this phase of a rolling pass. The controller design investigations in this work were aimed at a controller, which would regulate the process for a time fraction of the speed up ramp at 3.5 ± 0.2 m/s main drive

peripheral speed. From Fig. 3.2 it can be seen that this gives a controller 0.5 seconds to control the output variables back to within their limits specified in section 5.2.

For a functional control system during the speed up phase of a pass a whole set of controllers would be needed each operating at a different main drive speed. A control system, which coordinates the operation of every controller within this set, could be placed in the category of switching control systems.

In [37] a criterion for the switching time, at which a switching controller comes into action, is presented. According to [37] the switching time is determined from a bounding function and a norm of a vector of which the components are the switching controller states as well as filtered errors.

Given the abovementioned requirements for a switching controller the H_∞ controller for the second linear model qualifies as an element in a set of suitable switching controllers. The diagonal controller scheme can also be said to qualify as a suitable switching controller because it keeps the plant output variables within specified limits during the time available. The H_∞ controller for the third linear model however does not meet specification 5.2 iii) and therefore cannot be used as a switching controller.

Real plant data shows a severe exit gauge decrease (approximately 50 micrometers) as a result of the severe increase in front tension during the first moments of the speed up phase of the rolling pass [38].

6.7 Conclusion

Closed-loop simulations of the plant outputs and control actions have been shown for all three the controller schemes implemented on the nonlinear simulator. From the simulation graphs it became clear that the diagonal controller and the H_∞ controller for the second linear model comply with the requirements specified in 5.2.

The adverse effect of model mismatch can be seen in the performance of the diagonal controller and also in the excessive control action of the H_∞ controller for the third linear model.

With respect to the requirements for a switching controller it was found that the H_∞ controller for the second linear model is an option more suited than the other two controllers.